ACCSCIENCE PUBLISHING

International Journal of Bioprinting

RESEARCH ARTICLE

Hyaluronic acid-based self-healing hydrogels with enhanced hydrolytic stability for 3D bioprinting in tissue engineering

Minhyung Kong[1], Hyun Seung Kim[1], Jiwon Hwang[1], Joon Seo Park[1], In Young Lee[1], and Kuen Yong Lee[1,2]*

[1]Department of Bioengineering, Hanyang University, Seoul, Republic of Korea

[2]Institute for Bioengineering and Biopharmaceutical Research, Hanyang University, Seoul, Republic of Korea

(This article belongs to the *Special Issue*: *Future Bioprinting—Celebrating the 10th Anniversary of the International Journal of Bioprinting*)

Abstract

Hyaluronic acid (HA)-based hydrogels have gained significant interest for many biomedical applications because of their biocompatibility and degradability as glycosaminoglycans. However, it is challenging to control their mechanical properties and degradation rates. In this study, we investigated the potential of carbodihydrazide-modified HA (HA-CDH) and oxidized diol-modified HA (odHA) to form hydrogels. We modulated the mechanical stiffness of the HA-CDH/odHA hydrogels by adjusting the degree of CDH substitution and polymer composition in the gels. These hydrogels exhibited improved hydrolytic stability under physiological conditions, which was attributed to the presence of multiple delocalized electron arrangements within the hydrazone bonds. Notably, the enzymatic degradability of these hydrogels was unaffected by the hydrazone bonds. We developed self-healing HA-CDH/odHA hydrogels using free adipic acid dihydrazide and utilized them to fabricate various three-dimensional (3D) structures via 3D printing. We integrated resonance-stabilized hydrazone chemistry with self-healing behavior in HA-based hydrogels, enabling both slow degradation and direct extrusion-based 3D bioprinting of cell-laden constructs without secondary networks or post-crosslinking treatments. Furthermore, we investigated the effect of enhanced mechanical stiffness on *in vitro* cell differentiation and observed significant gene expression levels that were indicative of chondrogenic and osteogenic differentiation within hydrogels with increased stiffness. These findings could help elucidate the effect of the physical properties of natural polysaccharide-based hydrogels on cell phenotype modulation and expand their applications in tissue engineering.

***Keywords*:** 3D bioprinting; Hydrazide-modified hyaluronate; Hydrolytic degradation; Oxidized hyaluronate; Resonance structure; Self-healing

***Corresponding author:**
Kuen Yong Lee
(leeky@hanyang.ac.kr)

Citation: Kong M, Kim HS, Hwang J, Park JS, Lee IY, Lee KY. Hyaluronic acid-based self-healing hydrogels with enhanced hydrolytic stability for 3D bioprinting in tissue engineering. *Int J Bioprint*. 2025;11(6):374-389. doi: 10.36922/IJB025370372

Received: September 9, 2025
Revised: September 25, 2025
Accepted: October 1, 2025
Published online: October 2, 2025

1. Introduction

Hydrogels are defined as three-dimensional (3D) structures that contain crosslinked porous networks.[1] They are composed of hydrophilic polymers, which swell significantly

upon exposure to water or biological fluids.[2] Hydrogels are categorized into natural and synthetic hydrogels based on the origin of their constituent materials.[2,3] Hydrogels are highly biocompatible, and they closely resemble the macromolecular components found in the body. Thus, they are versatile materials with extensive applications in drug delivery and tissue engineering.[3,4] In tissue engineering, hydrogels play a pivotal role as synthetic extracellular matrices that are crucial for generating new tissues.[4,5] Polysaccharide-based hydrogels are typically used for this purpose owing to their biocompatibility and biodegradability.[6] However, the poor mechanical properties of hydrogels prepared using polysaccharides limit their potential applications in various biomedical fields.[7] To address this limitation, numerous strategies have been explored to enhance the mechanical properties of polysaccharide-based hydrogels, including the formation of multiple networks and the development of nanocomposite hydrogels.[8,9]

3D printing has recently emerged as a versatile method for fabricating complex structures, and it is widely used in tissue engineering.[10–12] This technique can be used to produce patient-specific scaffolds with precise shapes using computer-aided design.[13] Common 3D printing techniques include inkjet, extrusion-based, and laser-assisted printing.[14,15] However, conventional hydrogels are often unsuitable for extrusion-based 3D printing, as they may cause nozzle blockage, hinder effective material delivery, and lack the ability to recover their structures after printing.[16,17] Dynamic hydrogels are a new type of hydrogel, different from conventional hydrogels and highly promising for 3D printing. Their reversible crosslinking networks impart self-healing properties, shear-thinning behavior, and adaptability to environmental changes.[18,19] These characteristics enable dynamic hydrogels to recover their structure after extrusion and maintain high shape fidelity without the need for additional post-processing, making them particularly attractive for fabrication of complex, cell-laden structures. However, finding the optimal rheological properties for 3D printing—particularly achieving the right balance of stiffness, viscosity, and recovery speed without the application of external stimuli—remains challenging.[20]

Hyaluronic acid (HA) is a natural polysaccharide with exceptional water retention properties.[21] HA is widely used to prepare hydrogel scaffolds in tissue engineering owing to its excellent biocompatibility and nontoxic degradation products.[22] However, HA hydrogels exhibit rapid degradation rates and poor mechanical characteristics.[23] To overcome these drawbacks, various strategies have been explored to enhance gel stiffness and regulate degradation rates, including the use of dual crosslinking systems.[1,24-26] The formation of hydrazone bonds between HA derivatives introduces self-healing capabilities in resulting hydrogels.[27]

Hydrazone chemistry has been widely employed in hydrogels because of its reversible covalent crosslinking, which imparts dynamic properties such as self-healing, shear-thinning, and injectability. Hydrazone crosslinking can typically be carried out via a reaction between aldehydes and hydrazides, which serves as a dynamic crosslink.[28] These reactions have high reactivity, simple reaction conditions, no toxic reagents or side products, and high yields.[29] Modifying the polymer backbone by incorporating aldehyde or hydrazide groups provides potential crosslinking sites, influencing crosslinking kinetics and bond stability. Faster kinetics result from high concentrations of reactive groups or the use of catalysts like salts, while increased stability is achieved with more stable aromatic hydrazones or lower temperatures. Polymer backbone structure, such as the inherent length or presence of other functional groups, also impacts the reactivity of functional groups and the resulting network density, further controlling mechanical properties and dynamic behavior.[30] However, hydrazone bonds are reversible and prone to hydrolytic instability; this typically leads to rapid hydrogel degradation.[31,32]

In this study, we examined the potential of carbodihydrazide-modified HA (HA-CDH) combined with an aldehyde-containing HA derivative to form hydrogels with enhanced hydrolytic stability, which could be attributed to resonance structure formation within the acylhydrazone bond of the hydrogels (Figure 1). The presence of multiple delocalized electron arrangements within a hydrazone bond contributes to the enhanced stability.[31] We synthesized oxidized diol-modified HA (odHA) as an aldehyde-containing HA derivative because the oxidation of the HA backbone generates an open-chain adduct that is prone to hydrolysis.[33] Initially, a diol group was introduced to the HA side chain, followed by oxidation. This mitigates the significant reduction in the molecular weight of HA during the oxidation process and prevents the rapid degradation of the resulting hydrogels.[34] Additionally, we investigated whether the enzymatic degradation of HA-CDH/odHA hydrogels could be influenced by the resonance structure formation.

Given the significance of self-healing properties in facilitating the construction of 3D structures that encapsulate cells via 3D printing, we enhanced the self-healing capability of HA-CDH/odHA hydrogels using free adipic acid dihydrazide (ADH) through competitive acylhydrazone bond formation (Figure 1). Subsequently, we comprehensively investigated the characteristics of the HA-CDH/odHA/ADH hydrogels. Furthermore, we

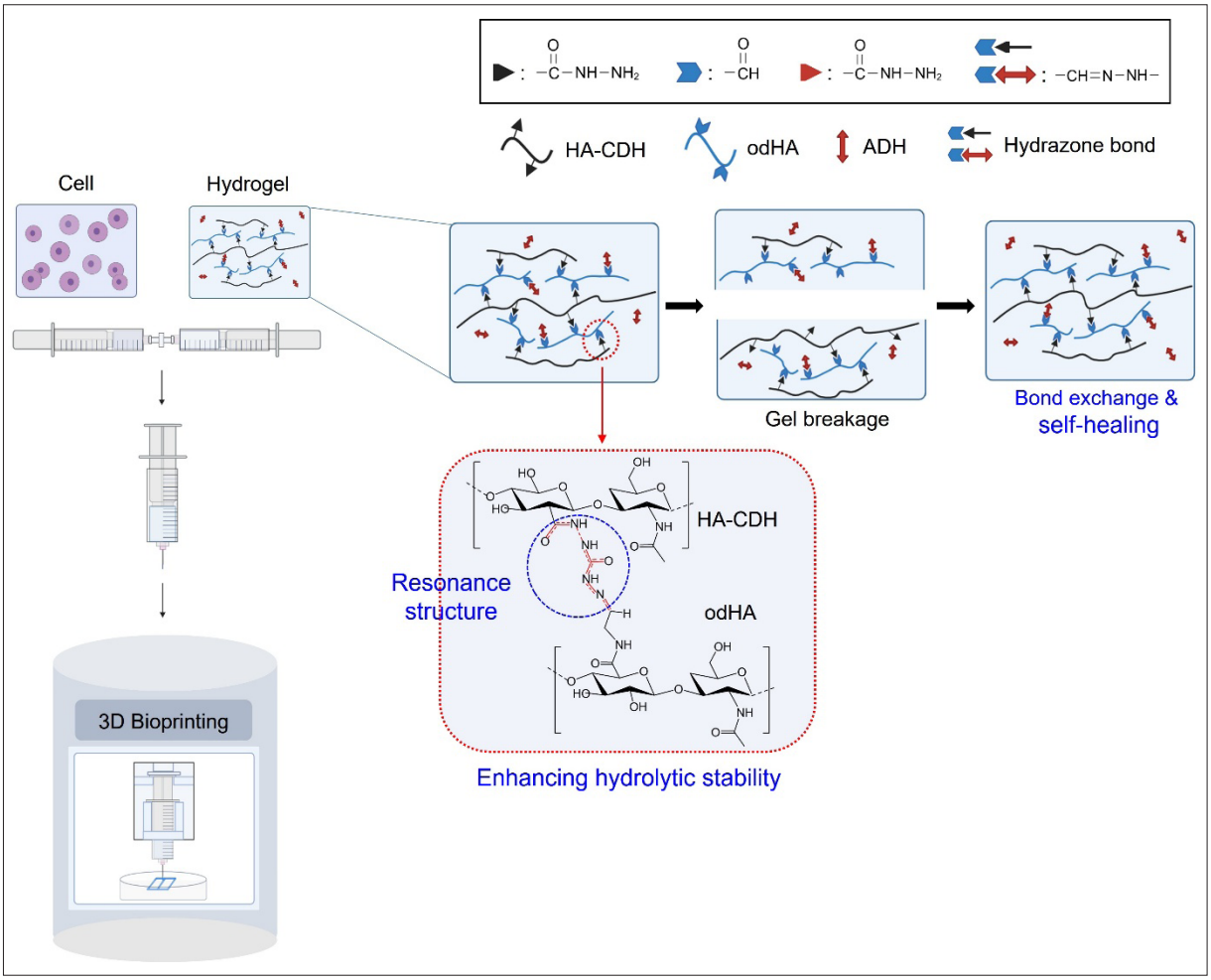

Figure 1. Schematic of 3D bioprinting of self-healing HA-CDH/odHA/ADH hydrogels with enhanced hydrolytic stability. Abbreviations: ADH, adipic acid dihydrazide; HA-CDH, carbodihydrazide-modified hyaluronic acid; odHA, oxidized diol-modified hyaluronic acid.

assessed the impact of the improved degradation and enhanced mechanical properties of the hydrogels on osteogenic and chondrogenic differentiation using *in vitro* experiments.

2. Materials and methods

2.1. Materials

Sodium hyaluronate (MW = 700 kDa) was purchased from Lifecore (Chaska, MN, USA). CDH, 3-amino-1,2-propanediol, and hyaluronidase were purchased from TCI (Tokyo, Japan). 1-Ethyl-3-(dimethylaminopropyl) carbodiimide (EDC) was purchased from Proteochem (Hurricane, UT, USA). *N*-hydroxysulfosuccinimide sodium salt (sulfo-NHS) was purchased from Covachem (Loves Park, IL, USA). Dulbecco's phosphate-buffered saline (DPBS), Dulbecco's modified Eagle's medium nutrient mixture F-12 (DMEM/F-12), minimum essential medium alpha (α-MEM), fetal bovine serum (FBS), and penicillin–streptomycin (PS) were purchased from Gibco (Grand Island, NY, USA). An EZ-Cytox kit was purchased from DoGenBio (Seoul, Korea). Alcian blue was purchased from Vector Laboratories (Newark, CA, USA), and Alizarin Red was purchased from ScienCell (Carlsbad, CA, USA). 2,4,6-Trinitrobenzene sulfonic acid (TNBSA) was purchased from Thermo Fisher Scientific (Waltham, MA, USA). 1-Hydroxybenzotriazole hydrate (HOBt), 2-(*N*-morpholino)ethanesulfonic acid (MES), ADH, and sodium chloride (NaCl) were purchased from Sigma-Aldrich (St. Louis, MO, USA). Sodium dodecyl sulfate (SDS) was purchased from Invitrogen (Waltham, MA, USA). Bovine serum albumin (BSA) was purchased from Amresco (Solon, OH, USA).

2.2. Synthesis of HA derivatives

HA-CDH was synthesized by first dissolving HA (1 g) in deionized water (0.5 wt.%) for 24 h. Then, HOBt (0.3567

g) and CDH (0.2375 g) were added to the HA solution ([HA]:[HOBt]:[CDH] = 1:1:1, molar ratio). EDC was added to the solution after 30 min ([EDC]:[CDH] = 0.1:1, molar ratio), and the pH was adjusted to 6. After 24 h, the reaction solution was dialyzed against 0.1 M NaCl, followed by additional dialysis in deionized water for 24 h (molecular weight cut-off = 3500 g/mol). The molar ratios of HA and CDH were varied ([HA]:[CDH] = 1:2 and 1:3, molar ratio) while maintaining a constant ratio between EDC and CDH ([EDC]:[CDH] = 0.1:1, molar ratio).

ADH-modified HA (HA-ADH) was also synthesized. HA was dissolved in a 0.1 M MES buffer (1 wt.%, pH 6.0), followed by reaction with ADH in the presence of EDC and sulfo-NHS for 24 h ([COOH]:[EDC]:[sulfo-NHS] = 1:0.65:0.65, molar ratio). Ethanol was used to precipitate HA-ADH, followed by lyophilization.[35]

odHA was synthesized by first dissolving HA (1 g) in deionized water (0.5 wt.%) for 24 h. Then, HOBt (0.3567 g) and 3-amino-1,2-propanediol (0.2 g) were added to the HA solution, and the pH was adjusted to 6. EDC (0.1515 g) dissolved in deionized water was added to the HA solution ([NH_2]:[HOBt]:[COOH] = 1:1:1, molar ratio) to synthesize diol-modified HA (dHA). After 24 h, the solution was dialyzed against dilute HCl (pH 3.5) containing 0.1 M NaCl for 48 h, followed by additional dialysis in deionized water for 24 h (molecular weight cut-off = 3500 g/mol) and lyophilization. The lyophilized dHA (1 g) was dissolved in deionized water for 24 h (0.5 wt.%) and partially oxidized with sodium periodate (0.56 g) for 10 min ([HA]/[$NaIO_4$] = 1:0.5, molar ratio). The reactant solution was treated with ethylene glycol (0.736 mL) to stop the oxidation reaction. The solution was dialyzed against deionized water for 48 h (molecular weight cut-off = 3500 g/mol) and lyophilized. All HA derivatives were stored at −20°C.[36]

2.3. Characterization of HA derivatives

The synthesis of the HA derivatives was verified through Fourier-transform infrared (FT-IR) spectroscopy (Nicolet6700, Thermo Fisher Scientific, Waltham, MA, USA). Samples were scanned over a wavenumber range of 600–2000 cm^{-1} (resolution = 4 cm^{-1}; scan rate = 4 mm/s). The TNBSA assay was used to quantify the degree of substitution (DS) of HA-CDH. The reaction buffer was prepared by adding sodium bicarbonate to deionized water and adjusting the pH to 8.5. Samples were dissolved in the reaction buffer (0.5 mL, 1 mg/mL), and a 0.01% TNBSA solution dissolved in the reaction buffer (0.25 mL) was added to the sample solution. Each sample was incubated at 37°C for 2 h, followed by the addition of 10% SDS (0.25 mL, 10%) and 1 N HCl (0.125 mL). The absorbance was measured at 340 nm, and the DS was calculated using BSA as the standard material. The odHA solution was treated with *t*-butyl carbazate, followed by a reaction with $NaCNBH_3$. The degree of aldehyde modification (%) of odHA was determined using ^1H nuclear magnetic resonance (NMR) spectroscopy (D_2O, VNMRS 600 MHz, Varian, Palo Alto, CA, USA).[34,35]

2.4. Determination of molecular weight

The molecular weights of HA derivatives were determined using size-exclusion chromatography with multiangle laser light scattering (SEC-MALLS). A Shimadzu system (Kyoto, Japan) equipped with a PL Aquagel-OH MIXED-H column (7.5 × 300 mm; Tosoh Bioscience, San Francisco, CA, USA), multiangle light scattering photometer, and differential refractometer (DAWN HELEOS || and Optilab Rex, Wyatt Technology, Santa Barbara, CA, USA) were used. Dextran was used as the standard polymer, and DPBS was employed as the mobile phase (flow rate: 0.5 mL/min). The dn/dc value of the HA derivatives was set as 0.167 mL/g.

2.5. Hydrogel fabrication and characterization

HA-CDH was dissolved in DPBS in the presence of free ADH for 24 h, followed by mixing with the odHA solution to form HA-CDH/odHA/ADH hydrogels. The ratio of HA-CDH to odHA was varied. HA-ADH was also used to prepare HA-ADH/odHA/ADH hydrogels. The viscoelastic properties of the hydrogels were determined using a rotational viscometer (Bohlin Gemini 150, Malvern, Worcestershire, UK; 5 Pa, 1 Hz) equipped with a parallel-plate fixture (diameter = 20 mm).

2.6. Hydrolytic stability test

Hydrogel disks (diameter = 10 mm, thickness = 1 mm) were immersed in DPBS and incubated at 37°C for 21 days. The diameter of each disk was determined using ImageJ (National Institutes of Health, USA) at predetermined time points. The changes in the dry weights of the disks were also measured after lyophilization.

2.7. Enzymatic stability test

Hydrogel disks (diameter = 10 mm, thickness = 1 mm) were immersed in DPBS containing hyaluronidase (1 μg/mL) and incubated at 37°C for 3 days. The gel disks were frozen and lyophilized before their dry weights were measured.

2.8. *In vitro* cell culture and cytotoxicity evaluation

ATDC5 cells (RIKEN Cell Bank, Tsukuba, Japan) were cultured in DMEM/F-12 supplemented with 5% FBS and 1% PS (37°C, 5% CO_2 atmosphere). MC3T3-E1 cells (RIKEN Cell Bank, Tsukuba, Japan) were cultured in α-MEM containing 10% FBS and 1% PS (37°C, 5% CO_2 atmosphere).

The *in vitro* cytotoxicity of soluble HA derivatives, sterilized using a 0.22-μm filter, was evaluated using the EZ-Cytox kit. In brief, the cells were seeded in a 96-well plate at a density of 5.0×10^3 cells/well and cultured. After 24 h of incubation, a sample solution (10 μL) was added to each well and incubated for 24 h. Then, the EZ-Cytox solution (10 μL) was added to each well and incubated for 4 h at 37°C. A spectrophotometer (SpectraMax M2e, Molecular Devices, Sunnyvale, CA, USA) was used to measure the absorbance at 450 nm. Cell viability was calculated relative to the absorbance of untreated cells.

2.9. Three-dimensional printing

An extrusion-based 3D printer (Invivo, Seoul, Korea) was used to construct various 3D structures. Hydrogels were placed in a 10 mL syringe and printed through a 25-gauge Teflon® needle (Rokit Healthcare, Seoul, Korea). The motor pressure was set as 300 N, and the infill density was fixed at 80%. The printing speed ranged from 5 to 15 mm/s. The shape fidelity of the 3D-printed cylindrical structures (diameter = 10 mm, height = 4 mm) was calculated by measuring the diameter and height after printing relative to the computer-designed structures. Various 3D structures were designed using Tinkercad (Autodesk, San Francisco, CA, USA) before printing.

The printability of the hydrogel was quantitatively assessed using a lattice structure. Square grids were printed at varying printing speeds, and the printed pore geometries were analyzed using ImageJ software. For each construct, the pore perimeter and area were measured, and the printability parameter (*Pr*) was calculated according to the following equation[37]:

$$Pr = \frac{(\text{Pore perimeter})^2}{16 \times \text{Pore area}}$$

A *Pr* value close to 1 indicates that the printed pore closely approximates an ideal square shape, whereas a value deviating from 1 reflects structural distortion.

2.10. Cell viability within hydrogel after printing

Cells (1×10^6 cells/mL) were mixed with the odHA solution and then mixed with the HA-CDH/ADH solution to form cell-encapsulated HA-CDH/odHA/ADH hydrogels. HA-CDH and odHA solutions were prepared in DPBS. The resulting cell-laden hydrogels were immediately placed in culture plates, covered with fresh medium, and incubated at 37°C in a 5% CO_2 atmosphere. The cell viability within the hydrogels before and after printing was evaluated using a live/dead assay kit (Invitrogen). Ethidium homodimer-1 (20 μL) and calcein AM (5 μL) in DPBS (10 mL) were added to the cell-encapsulating hydrogels. Confocal microscopy was used to obtain images (LSM 900, Carl Zeiss, Germany) at the Biospecimen-Multiomics Digital Bioanalysis Core Facility of Hanyang University.

2.11. *In vitro* histological analysis and gene expression

ATDC5 or MC3T3-E1 cells were encapsulated in the hydrogels at a density of 5×10^6 cells/mL and incubated at 37°C in a 5% CO_2 atmosphere for 14 days. Then, the hydrogels were embedded in a Tissue Tek® O.C.T. compound (Sakura Finetech, Torrance, CA, USA), frozen using liquid nitrogen, and cut to a thickness of 12 μm using a cryostat (Leica Biosystems, Nußloch, Germany). The hydrogel sections were stained with Alcian blue and Alizarin red for ATDC5 and MC3T3-E1 cells, respectively.

The chondrogenic differentiation of ATDC5 cells and osteogenic differentiation of MC3T3-E1 cells were quantified by means of quantitative polymerase chain reaction (PCR) analysis. The hydrogel constructs were homogenized, and RNA was retrieved using an RNAiso Plus kit (Takara, Kusatsu, Japan). The gene expression levels of SRY-box transcription factor 9 (*SOX9*), collagen type 2 (*COL2*), osteopontin (*OPN*), osteocalcin (*OCN*), and collagen type 1 (*COL1*) were quantified through comparison with that of β-actin using an ABI PRISM 7500 Real-Time PCR system (Applied Biosystems, Grand Island, NY, USA) and SensiMax SYBR (Bioline, Memphis, TN, USA).

The following primer sequences were used for ATDC5 (Cosmogenetech, Seoul, Korea): *β-actin*, (*forward*) 5′−CCCTGAACCCTAAGGCCAAC-3′, (*reverse*) 5′-GCATACAGGGACAGCACAGC-3′; *SOX-9*, (*forward*) 5′-AAGTCGGAGAGCCGAGAGCG-3′, (*reverse*) 5′-ACGAAACCG GGGCCACTTGC-3′; *COL2*, (*forward*) 5′-CACACTGGTAAGTGGGGCAAGACCG-3′, 5’-GGATTGTGTT GTTTCAGGGTTCGGG-3′.

The following primer sequences were used for MC3T3-E1 (Cosmogenetech, Seoul, Korea): *β-actin*, (*forward*) 5′-GTATCCTCGGATGTTGCTGCCTTG-3′, (*reverse*) 5′-CGCTGAGCATTGGTCCTCTTGG-3′; *OCN*, (*forward*) 5′-CGCCTACAAACGCATCTACG-3′, (*reverse*) 5′-CAGAGAGAGAGGACAGGGAGGA-3′; *COL1*, (*forward*) 5′-GACATGTTCAGCTTTGTGGACCTC-3′, (*reverse*) 5′-GGGACCCTTAGGCCATTGTGTA-3′.

2.12. Statistical analysis

All data are expressed as mean and standard deviation ($n = 4$). The Student's *t*-test was used to evaluate statistical significance. A *p*-value less than 0.05 was considered statistically significant.

3. Results and discussion

3.1. Synthesis and characterization of HA-CDH and odHA

HA-CDH was synthesized by coupling CDH with HA via carbodiimide chemistry. The hydrazide groups in HA-CDH enabled the formation of hydrazone bonds with the aldehyde group of odHA (Figure 2). The conjugation of CDH to HA was confirmed through FT-IR spectroscopy (Figure S**1**). A new peak was observed at 1710 cm^{-1} (C=O stretching), which corresponded to the formation of hydrazide groups between HA and CDH.[24,38] Various HA-CDH derivatives were synthesized by varying the amount of CDH used in the reaction with HA. The DS of CDH in HA-CDH was determined using the TNBSA assay. The theoretical and actual DS values are listed in Table 1. The conjugation efficiency was >85% for all HA-CDH derivatives used in this study. The number following HA-CDH indicates the theoretical DS. The actual DS of HA-ADH50 was determined using ^{1}H NMR spectroscopy. The peak areas of the acetamido moiety (**1**) and ADH (**3, 4**) of HA-ADH50 (Figure S2) were integrated to calculate the DS, which was found to be 46%.

The presence of aldehyde groups in odHA was confirmed using FT-IR spectroscopy (Figure S1). A clear peak was observed at 1730 cm^{-1} (C=O stretching, aldehyde).[39] The degree of aldehyde modification of odHA was determined to be 20% using ^{1}H NMR spectroscopy. The peak areas of the acetamido (**1**) and *t*-butyl (**2**) moieties of odHA in ^{1}H NMR spectra were integrated to calculate the number of aldehyde groups present (Figure S2). The molecular weight of odHA, as determined by SEC-MALLS, showed no significant decrease compared with that of intact HA. This indicated that the HA backbone was maintained during oxidation. This is in contrast to the oxidation of C2–C3 diols in the pyranose ring of HA, which typically leads to a reduction in the molecular weight. The molecular weights of HA-CDH are listed in Table 2. No significant changes in the molecular weights were observed for most types of HA-CDH, except for HA-CDH30.

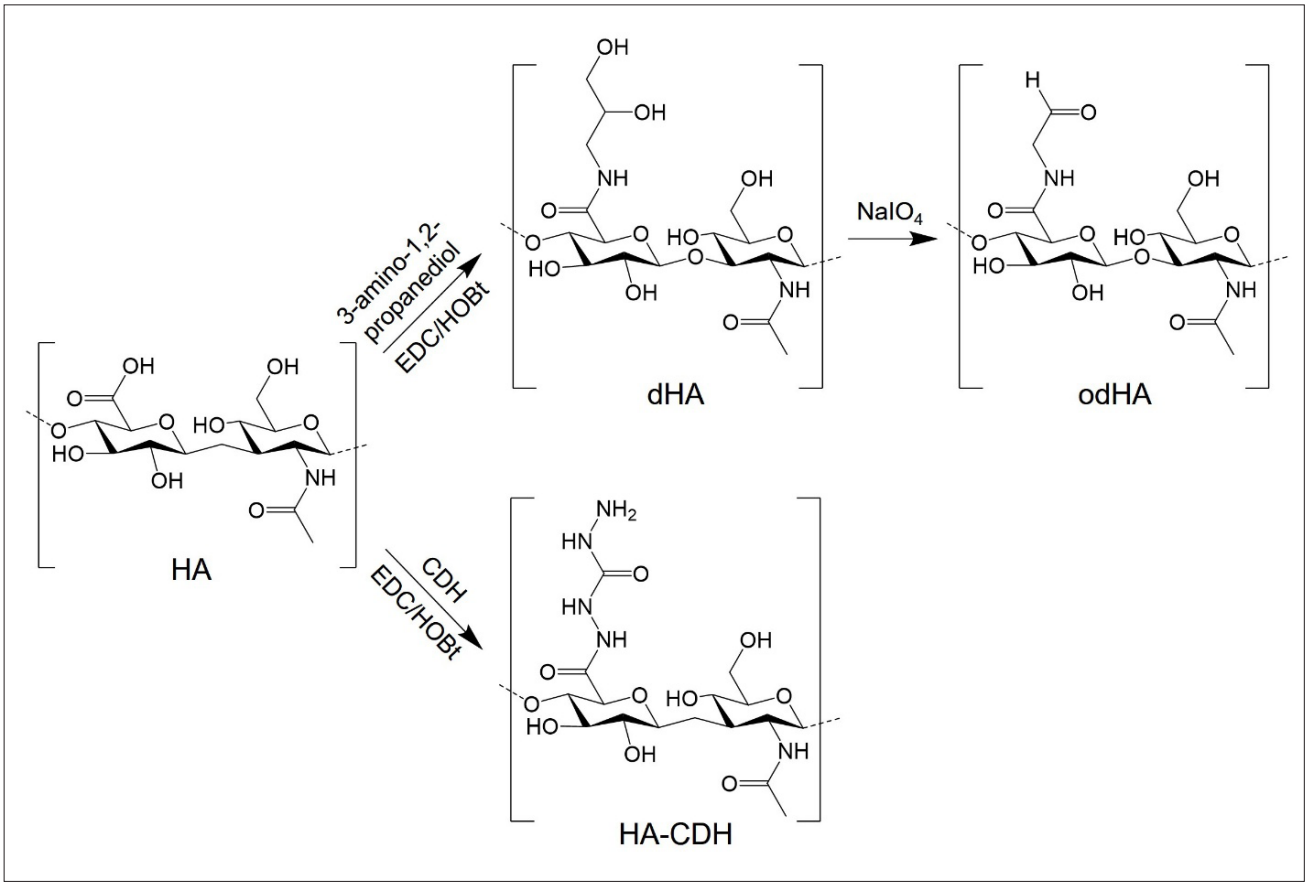

Figure 2. Chemical structures of HA, dHA, odHA, and HA-CDH. Abbreviations: CDH, carbodihydrazide; dHA, diol-modified hyaluronic acid; EDC, 1-ethyl-3-(dimethylaminopropyl) carbodiimide; HA: hyaluronic acid; HA-CDH, carbodihydrazide-modified hyaluronic acid; HOBt, 1-hydroxybenzotriazole hydrate; odHA, oxidized diol-modified hyaluronic acid.

Table 1. Conjugation efficiency and theoretical DS of HA-CDH

Sample[a]	Theoretical DS (%)	Actual DS (%)	Conjugation efficiency (%)
HA-CDH10	10	8.6	86.4
HA-CDH20	20	18.7	93.7
HA-CDH30	30	25.4	84.9

Note: [a]The number after the term 'HA-CDH' indicates the theoretical DS value.

Abbreviations: DS, degree of substitution; HA-CDH, carbodihydrazide-modified hyaluronic acid.

Table 2. Molecular weights of HA derivatives used in this study

Sample	M_w[a] (g/mol)
HA	5.0×10^5
HA-CDH10	5.7×10^5
HA-CDH20	5.7×10^5
HA-CDH30	7.1×10^5
HA-ADH50	5.8×10^5
odHA	4.6×10^5

Note: [a]Weight-average molecular weight determined via SEC-MALLS measurements.

Abbreviations: HA, hyaluronic acid; HA-CDH, carbodihydrazide-modified hyaluronic acid; M_w, molecular weight; odHA, oxidized diol-modified hyaluronic acid; SEC-MALLS, size-exclusion chromatography with multiangle laser light scattering.

The cytotoxicity of the HA-CDH and odHA solutions was evaluated *in vitro* using ATDC5 and MC3T3-E1 cells (Figure S3). The viability of MC3T3-E1 cells was not significantly affected by treatment with the soluble forms of HA-CDH and odHA. However, the number of ATDC5 cells treated with high concentrations of HA-CDH30 was slightly reduced. This suggested that the component polymers of the hydrogels were not cytotoxic. However, high concentrations of certain derivatives, such as HA-CDH30, might have adversely affected specific cell types. Free ADH also did not significantly affect the cytotoxicity.[40]

3.2. Preparation and characterization of hydrogels

The solutions of HA-CDH and odHA in DPBS were thoroughly mixed at room temperature to form hydrogels. An increase in the DS of CDH in HA-CDH enhanced the storage shear modulus (G′) values of the HA-CDH/odHA hydrogels at the same polymer concentration ([HA-CDH] = 1.5 wt.%, [odHA] = 1.0 wt.%). Although the HA-CDH30/odHA hydrogel exhibited the highest value of G′ (Figure 3A), inhomogeneous gel formation was observed. Furthermore, complete dissolution was not achieved when HA-CDH was dissolved in DPBS at 2 wt.%, regardless of the DS. As a result, HA-CDH20 at 1.5 wt.% was selected and used for further experiments because of homogeneous gel-forming capability. The concentration of odHA also influenced gel formation and the resultant viscoelastic properties of the gel. The value of G′ for the HA-CDH20/odHA hydrogels increased with the odHA concentration at [HA-CDH20] = 1.5 wt.% (Figure 3B). However, rapid gelation prevented complete hydrogel formation at [odHA] = 1.5 wt.%. Thus, [odHA] = 1 wt.% was employed for further gel preparation.

Although the hydrazone bond in the HA-CDH20/odHA hydrogel was reversible, it did not exhibit self-healing behavior. To address this, free ADH was added to the hydrogel to induce competitive hydrazone bond formation with the bond between HA-CDH and odHA. The minimum concentration of free ADH required for the self-healing of the HA-CDH20/odHA hydrogel was determined to be 0.1 wt.%, as confirmed by rotational viscometer measurements (data not shown). However, the value of G′ for the HA-CDH20/odHA hydrogel decreased as the ADH concentration in the gel increased (Figure 3C). Therefore, [ADH] = 0.1 wt.% was used to prepare the self-healing HA-CDH20/odHA/ADH hydrogel.

Hydrogels were also prepared using HA-ADH50 as the conventional hydrazone-based dynamic hydrogels, which had a DS similar to that of HA-CDH20. The value of G′ for the HA-CDH20/odHA/ADH hydrogel was considerably higher than that for the HA-ADH50/odHA/ADH hydrogel (Figure 3D). HA-ADH50 was synthesized as previously reported and used to form hydrogels (Figure S4).[34,35] HA-ADH with varying degrees of hydrazide substitution was synthesized and crosslinked with oxidized HA to form self-healing hydrogels, which showed potential for 3D bioprinting. However, these hydrogels exhibited rapid degradation under physiological conditions. To address this limitation, we designed HA-CDH-based hydrogels with improved resistance to degradation.

HA can be chemically tailored by introducing complementary aldehyde and hydrazide moieties, which are crosslinked through hydrazone bond formation. Incorporation of these reactive groups onto the polymer backbone generates sites for covalent bonding, thereby affecting both the rate of crosslinking and the stability of the resulting network. Reaction kinetics are typically

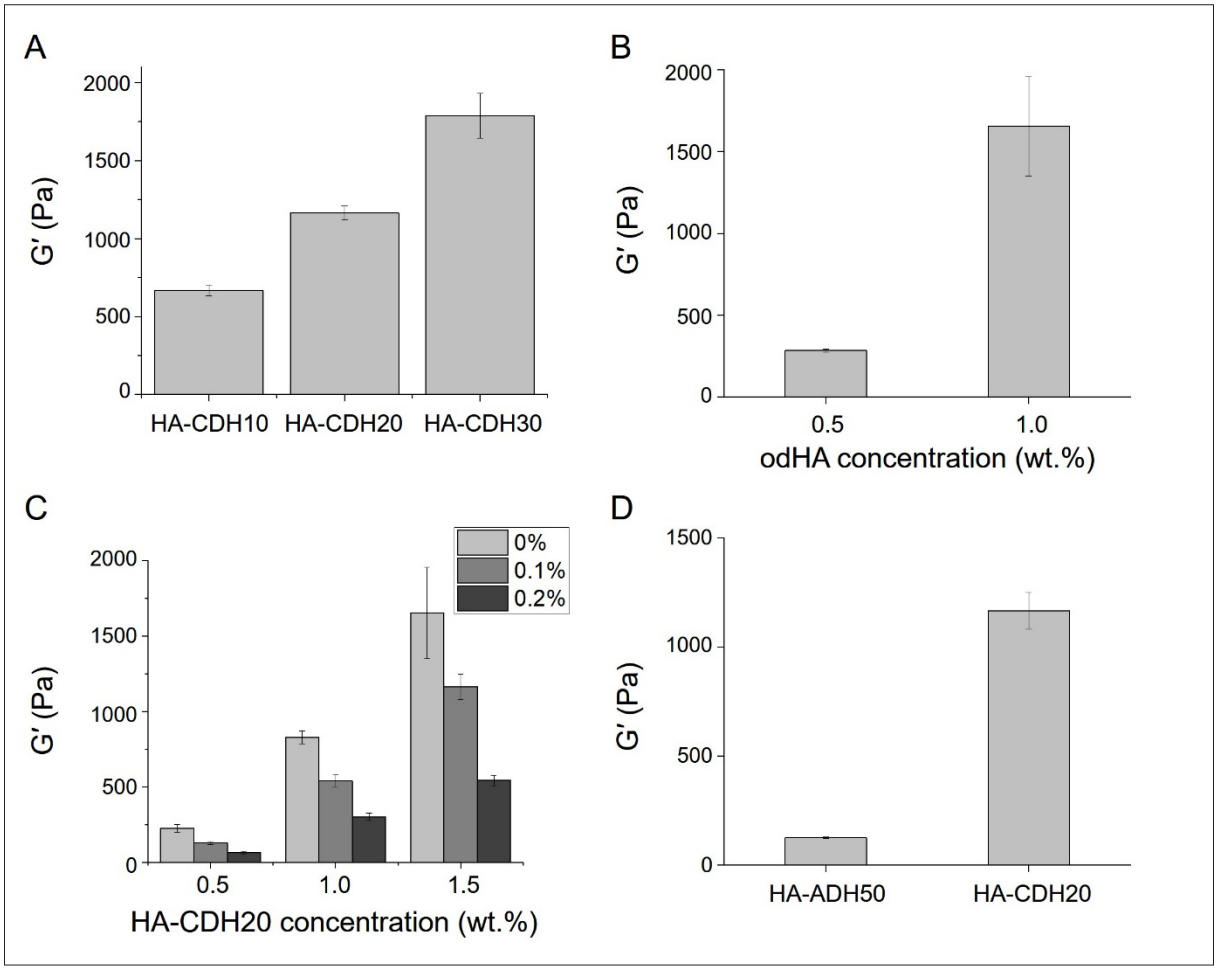

Figure 3. Viscoelastic properties of hydrogels. (A) Storage shear modulus (G′) of HA-CDH/odHA hydrogels prepared using various types of HA-CDH ([HA-CDH] = 1.5 wt.%, [odHA] = 1.0 wt.%). (B) Values of G′for HA-CDH20/odHA hydrogels at different odHA concentrations ([HA-CDH20] = 1.5 wt.%). (C) Values of G′ for HA-CDH20/odHA/ADH hydrogels containing different amounts of HA-CDH20 and ADH ([odHA] = 1.0 wt.%). (D) Values of G′ for hydrogels containing either HA-ADH50 or HA-CDH20 ([HA-ADH50] = 1.5 wt.%, [HA-CDH20] = 1.5 wt.%, [odHA] = 1 wt.%, [ADH] = 0.1 wt.%). Abbreviations: ADH, adipic acid dihydrazide; HA-ADH, adipic acid dihydrazide-modified hyaluronic acid; HA-CDH, carbodihydrazide-modified hyaluronic acid; odHA, oxidized diol-modified hyaluronic acid.

accelerated when the density of functional groups is high or when catalytic agents are present. The structural characteristics of the polymer backbone—including chain length and the presence of other substituents—also influence functional group reactivity, network density, and ultimately the mechanical strength and dynamic behavior of the hydrogel.[30] Moreover, the valency of the crosslinker is another critical factor; for instance, shifting from a divalent to a tetravalent crosslinker has been shown to move the strain-stiffening response into biologically relevant ranges.[41]

3.3. Self-healing properties of hydrogels

The self-healing behavior of the HA-CDH20/odHA/ADH hydrogel was confirmed macroscopically. When the gel was deliberately broken into two pieces and subsequently reattached, the cracks disappeared within 30 min (Figure 4A). This self-healing property was validated using a rotational viscometer. An amplitude sweep was performed to determine the gel flow point (157% strain), which was defined as the intersection point of G′ and G″; this point indicated gel breakage (Figure 4B). During repeated cycles of strain variation from 1% to 500%, G″ became higher than G′ at 500% strain because of gel breakage. However, G′ increased again when strain was reduced to 1%, demonstrating the self-healing properties of the hydrogel (Figure 4C).

Self-healing was achieved through the competitive reaction of free ADH and CDH in HA-CDH, both of which contained the dihydrazide group, with odHA. This resulted in the formation of reversible and dynamic

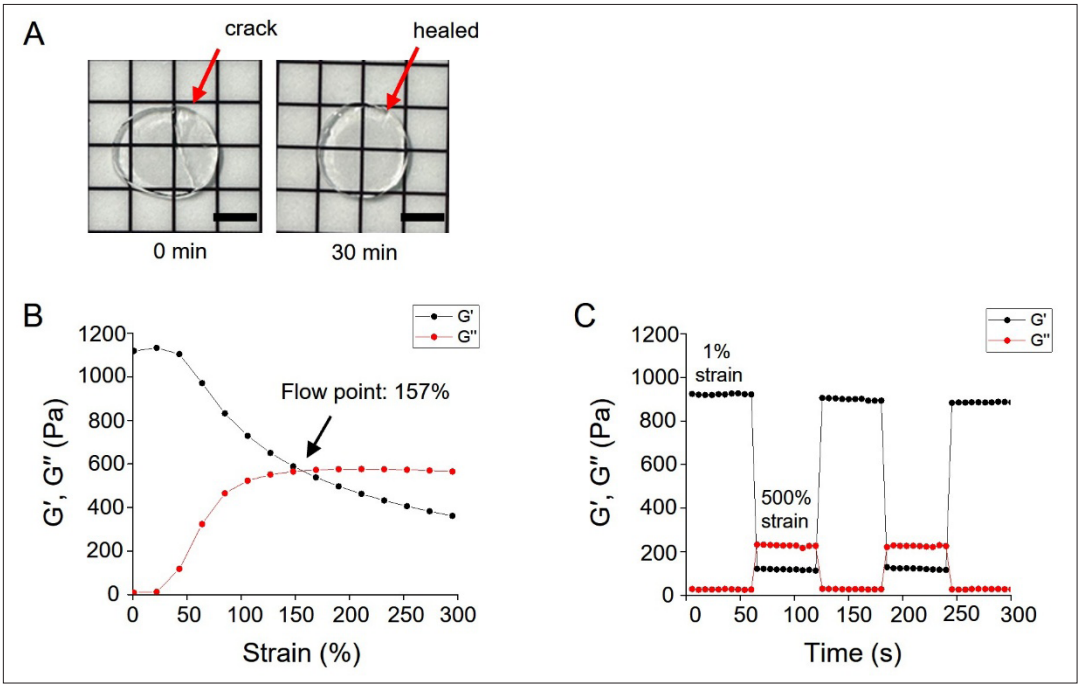

Figure 4. Self-healing properties of hydrogels. (A) Self-healing behavior of HA-CDH20/odHA/ADH hydrogel. The arrows indicate the location of the deliberately induced crack, which self-heals after 30 min (scale bar: 5 mm). (B) Amplitude sweep to determine the flow point of HA-CDH20/odHA/ADH hydrogel and (C) repeated self-healing behavior of the hydrogel ([HA-CDH20] = 1.5 wt.%, [odHA] = 1 wt.%, [ADH] = 0.1 wt.%). Abbreviations: ADH, adipic acid dihydrazide; HA-CDH, carbodihydrazide-modified hyaluronic acid; odHA, oxidized diol-modified hyaluronic acid.

hydrazone bonds. This self-healing property is crucial for the extrusion-based 3D printing of hydrogels as bioinks because it enables the hydrogels to retain their integrated morphology without any additional treatment after printing.[20,42] Without free ADH, the self-healing of HA-CDH/odHA hydrogels was incomplete, with a recovery rate of approximately 75%, making them unsuitable for extrusion-type 3D printing. Importantly, essential requirements for bioinks include shear-thinning behavior, self-healing ability, and rapid recovery of a gel state ($G' > G''$) after extrusion.[43]

3.4. Enhanced hydrolytic stability of hydrogels

The hydrolytic stability of the HA-CDH/odHA/ADH hydrogels was investigated. Hydrogel disks were immersed in DPBS and incubated at 37°C, and the changes in the gel disk diameter were monitored for 21 days. The HA-CDH20/odHA/ADH hydrogel maintained its stability for 21 days. In contrast, the HA-ADH50/odHA/ADH hydrogel rapidly lost its integrity and completely disintegrated within 3 days, even though it contained the same number of aldehyde and hydrazide groups (Figure 5A). The enhanced stability of the HA-CDH20/odHA/ADH hydrogel was attributed to the ability of CDH to form resonance structures when bound to an aldehyde group.[27] Resonance structures were formed when HA-CDH was mixed with odHA, which increased the stability of the hydrogel against hydrolysis (Figure 5B). The presence of multiple delocalized electron arrangements within the hydrazone compound contributed to the enhanced stability. These HA-CDH20/odHA/ADH hydrogels retained their self-healing properties during degradation, indicating preservation of dynamic hydrazone bonds during the process.

In contrast, the HA-ADH50/odHA/ADH hydrogel lacked the resonance structure formation between HA-ADH50 and odHA, leading to rapid disintegration. This was because the hydrocarbon groups in the middle impeded electron movement, thus preventing the formation of resonance structures (Figure S5). The changes in the weights of the hydrogel disks were monitored over time. The HA-ADH50/odHA/ADH hydrogel rapidly lost weight in DPBS at 37°C. In contrast, the HA-CDH/odHA/ADH hydrogel maintained its weight over time (Figure S6).

It should be noted that the HA-CDH20/odHA/ADH hydrogel was degraded by hyaluronidase (Figure 5C). HA was cleaved by hyaluronidase into smaller oligosaccharide fragments,[44] and the HA-CDH20/odHA/ADH hydrogel was similarly degraded by hyaluronidase. This finding clearly indicated that the introduction of CDH into HA contributed solely to the hydrolytic stability of the resultant

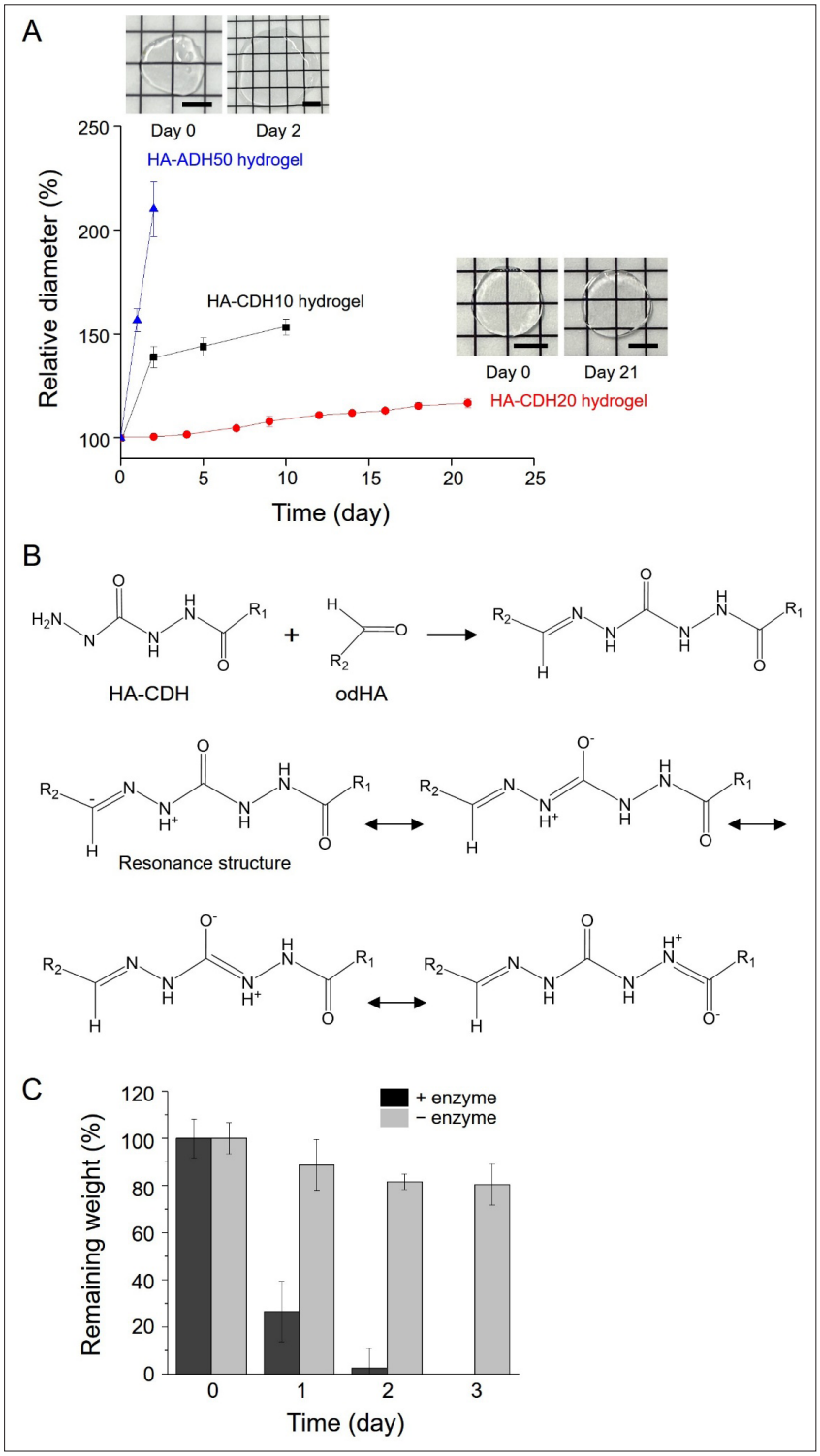

Figure 5. Degradation behavior of hydrogels. (A) Changes in the diameters of various hydrogel disks incubated at 37°C in DPBS over time, as compared with the initial diameters before incubation. Representative images of HA-CDH20/odHA/ADH and HA-ADH50/odHA/ADH hydrogels are included. (B) Possible resonance structures of the hydrazone bond formed between HA-CDH and odHA. (C) Changes in the remaining weights of HA-CDH20/odHA/ADH hydrogels incubated at 37°C in DPBS over time in the presence and absence of hyaluronidase. The remaining dry weight is compared with that before incubation ([HA-CDH20] = 1.5 wt.%, [odHA] = 1 wt.%, [ADH] = 0.1 wt.%, [hyaluronidase] = 1 μg/mL). Abbreviations: ADH, adipic acid dihydrazide; DPBS, Dulbecco's phosphate-buffered saline; HA-ADH, adipic acid dihydrazide-modified hyaluronic acid; HA-CDH, carbodihydrazide-modified hyaluronic acid; odHA, oxidized diol-modified hyaluronic acid.

HA-CDH/odHA/ADH hydrogels and did not interfere with their enzymatic degradability.

It is critical to control the hydrolytic stability of hydrogels because tissue scaffolds must maintain their mechanical integrity to match the rate of tissue regeneration, which varies depending on the tissue type. Conventional self-healing hydrogels are prone to hydrolytic degradation owing to reversible crosslinking. However, HA-CDH prevents the rapid degradation observed in HA-based self-healing hydrogels, which typically employ reversible hydrazone bonds.

3.5. Three-dimensional printing

An extrusion-based 3D printer was used to test the printing capability of the HA-CDH20/odHA/ADH hydrogel. The self-healing capability of the hydrogel allowed for extrusion-based 3D printing because the hydrogel retained its integrated morphology after printing without any additional process. The optimum printing speed was determined by assessing filament diameter, printability, and shape fidelity. As the printing speed increased, the filament diameter significantly decreased. The printed filament maintained an appropriate linear shape at printing speeds of 5 and 10 mm/s. However, the filament occasionally broke along its length at 15 mm/s (Figure 6A).

The printability of the hydrogel was quantitatively evaluated at varying printing speeds. The morphology of the printed lattice pores remained generally consistent across conditions, though minor deviations were noted. At 5 and 10 mm/s, the *Pr* values were close to 1, indicating good preservation of the designed square geometry. In contrast, the *Pr* value decreased slightly at 15 mm/s,

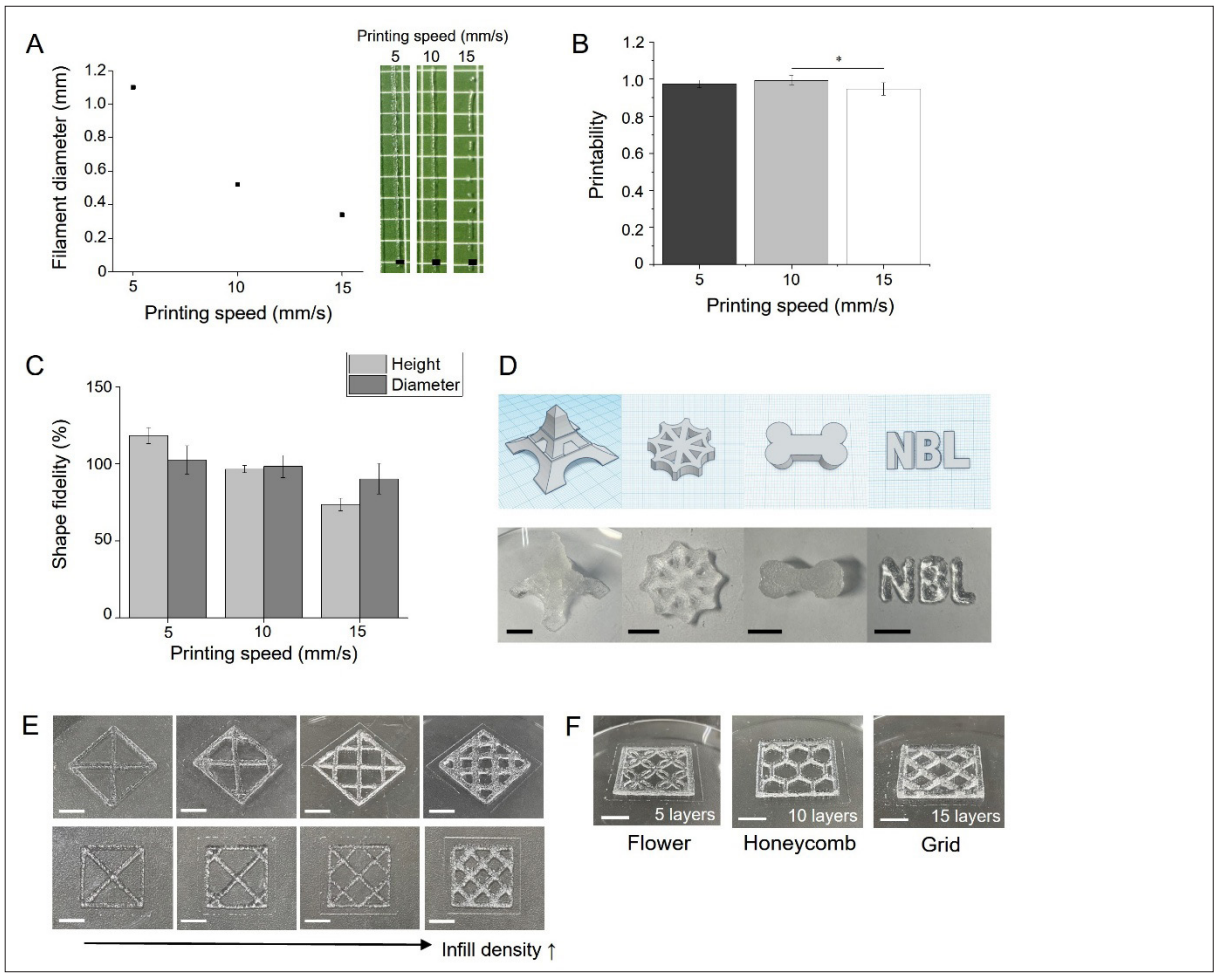

Figure 6. Three-dimensional printing of hydrogels. (A–C) Effects of printing speed on filament diameter (scale bar: 2 mm) (A), printability (B), and shape fidelity (C) for 3D printing using HA-CDH20/odHA/ADH ([HA-CDH20] = 1.5 wt.%, [odHA] = 1 wt.%, [ADH] = 0.1 wt.%; $^*p < 0.05$). (D) Various 3D structures printed using HA-CDH20/odHA/ADH hydrogel (scale bar: 10 mm). (E and F) Changes in infill density (E) and infill pattern (F) of 3D-printed constructs (scale bar: 10 mm). Abbreviations: ADH, adipic acid dihydrazide; HA-CDH, carbodihydrazide-modified hyaluronic acid; odHA, oxidized diol-modified hyaluronic acid.

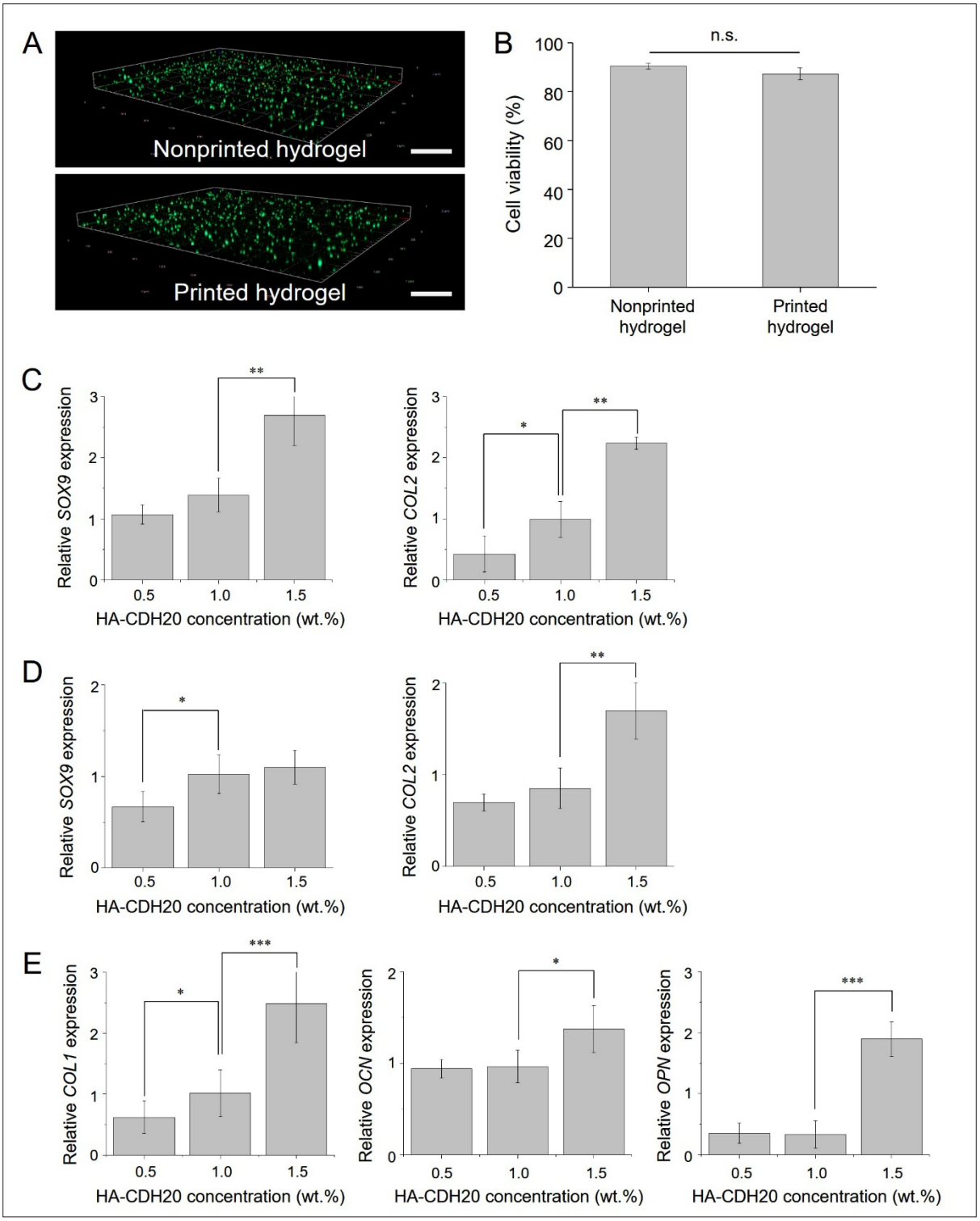

Figure 7. Cell viability and differentiation in hydrogels. (A and B) Confocal microscopy images of HA-CDH20/odHA/ADH hydrogels encapsulating ATDC5 cells after 24 h of culture (A) and their quantitative results (scale bar: 500 μm; n.s.: no statistical significance) (B). (C and D) Quantitative analysis performed on gene expression levels of ATDC5 cells cultured for 7 days (C) and 14 days (D) within HA-CDH20/odHA/ADH hydrogels prepared using various HA-CDH20 concentrations. (E) Quantitative gene expression levels of MC3T3-E1 cells cultured within HA-CDH20/odHA/ADH hydrogels for 14 days (*$p < 0.05$, **$p < 0.01$, ***$p < 0.001$). Abbreviations: ADH, adipic acid dihydrazide; HA-CDH, carbodihydrazide-modified hyaluronic acid; odHA, oxidized diol-modified hyaluronic acid.

reflecting reduced geometric fidelity at higher speeds (Figures 6B and S7).

The shape fidelity was tested by printing a gel disk with a diameter of 10 mm and a height of 4 mm and assessing the accuracy of reproducing these dimensions (Figure 6C). The diameter was close to that of the original design at printing speeds of 5 and 10 mm/s. However, at 5 mm/s, the height increased owing to filament accumulation at a single location. In contrast, the diameter and height of the printed constructs slightly decreased at 15 mm/s. Based on these results, a printing speed of 10 mm/s was selected for further experiments, as it produces lattices with uniform pore geometry, sharp corners, and well-aligned strands.

Various shapes of 3D constructs were designed and printed (Figure 6D). Additionally, adjustable infill density and various infill patterns of 3D-printed constructs were achieved at the optimized printing speed (Figure 6E and F).

3.6. *In vitro* cell differentiation within 3D constructs

Cell viability within the 3D-printed constructs was evaluated. 3D structures encapsulating ATDC5 cells were printed, and their viability was assessed using confocal microscopy (Figure 7A). No significant cytotoxicity was observed within the printed and nonprinted hydrogels 24 h after printing (Figure 7B). This suggested that 3D bioprinting with the HA-CDH20/odHA/ADH hydrogel did not significantly influence cell viability during the printing process and could be a suitable method for fabricating 3D constructs containing cells.

Cellular differentiation is generally affected by matrix stiffness.[45–47] To test the effect of the hydrogel stiffness on chondrogenic and osteogenic differentiation, HA-CDH20/odHA/ADH hydrogels with various HA-CDH20 concentrations ([HA-CDH20] = 0.5–1.5 wt.%) were used to encapsulate either ATDC5 or MC3T3-E1 cells. The chondrogenic differentiation of ATDC5 cells was investigated by quantifying the expression levels of *SOX9* and *COL2* as representative marker genes on days 7 (Figure 7C) and 14 (Figure 7D) after incubation. The osteogenic differentiation of MC3T3-E1 cells was also assessed by quantifying the expression levels of *OCN*, *OPN*, and *COL1* as representative marker genes on day 14 after incubation (Figure 7E). The chondrogenic and osteogenic differentiation of cells were affected by the gel stiffness of the HA-CDH20/odHA/ADH hydrogels induced by varying the HA-CDH20 concentration. The gene expression levels were significantly higher when cells were encapsulated and cultured within HA-CDH20/odHA/ADH hydrogels at [HA-CDH20] = 1.5 wt.% as compared with other groups. This was attributed to the enhanced gel stiffness (Figure 3C). Additionally, the hydrogel sections stained with Alcian blue and Alizarin red supported the pronounced differentiation of ATDC5 or MC3T3-E1 cells cultured within the HA-CDH20/odHA/ADH hydrogels at [HA-CDH20] = 1.5 wt.% (Figure S8).

Matrix stiffness generally controls the cell phenotype, including cell differentiation.[24,45] Thus, hydrogel stiffness significantly influences cell phenotype in tissue engineering approaches. Hydrogel stiffness is typically regulated by controlling the crosslinking density. In this study, the DS of HA-CDH and the concentrations of HA-CDH and odHA in the hydrogels were varied to change the crosslinking density and mechanical stiffness of the resultant gels. Hydrogels should maintain their stiffness and integrity for the required time and ideally match the rate of tissue formation during tissue regeneration. Hydrogel degradation can also be affected by the crosslinking density. However, crosslinking between the hydrazide-modified and aldehyde polymers results in hydrolysable hydrazone bonds in the gel network. The use of CDH in this study significantly reduced the hydrolytic degradation of the HA-CDH/odHA hydrogels owing to the formation of a resonance structure between the crosslinks. This approach of controlling gel stiffness and degradation rate while maintaining self-healing features can be widely utilized for the 3D bioprinting of complex tissue constructs in various tissue engineering applications.

4. Conclusion

In the present study, we demonstrated that: (i) tunable mechanical stiffness can be achieved through controlled CDH substitution and polymer composition; (ii) hydrolytic stability can be significantly enhanced without compromising enzymatic degradability; and (iii) successful fabrication of cell-laden constructs can support both chondrogenic and osteogenic differentiation. HA-based hydrogels with improved mechanical properties and degradation behaviors were successfully synthesized in this study. The combination of HA-CDH and odHA enhanced the hydrolytic stability of the resulting hydrogels, and the addition of free ADH conferred effective self-healing properties to the gels. These hydrogels with tailored DS and polymer concentration could simultaneously achieve slow degradation via CDH-mediated resonance stabilization and robust self-healing properties, which were suitable for extrusion-based 3D printing under optimal conditions. This study also highlighted the influence of enhanced mechanical stiffness on *in vitro* cell differentiation, suggesting the potential of these hydrogels for tissue engineering applications, particularly in cartilage and bone regeneration. These findings address

the limitations associated with the stability and mechanical properties of natural polysaccharide-based hydrogels. In addition, integrating these hydrogels with advanced bioprinting strategies, such as multi-material printing or integration with vascularization approaches, could further accelerate their translational potential in regenerative medicine. Overall, this platform lays the groundwork for the development of next-generation bioinks designed for personalized tissue engineering applications.

Acknowledgments

None.

Funding

This study was supported by the National Research Foundation of Korea (NRF) grant funded by the Korean Government (MSIT) (RS-2024-00355200).

Conflict of interest

The authors declare they have no competing interests.

Author contributions

Conceptualization: Minhyung Kong, Kuen Yong Lee
Investigation: Minhyung Kong, Hyun Seung Kim, In Young Lee
Methodology: Minhyung Kong, Jiwon Hwang, Joon Seo Park
Writing–original draft: Minhyung Kong
Writing–review & editing: Kuen Yong Lee

Ethical approval and consent to participate

Not applicable.

Consent for publication

Not applicable.

Availability of data

Data are available from the corresponding author upon reasonable request.

References

1. Ahmed EM. Hydrogel: preparation, characterization, and applications: a review. *J Adv Res.* 2015;6(2):105-121. doi:10.1016/j.jare.2013.07.006.

2. Zhu T, Mao J, Cheng Y, *et al.* Recent progress of polysaccharide-based hydrogel interfaces for wound healing and tissue engineering. *Adv Mater Interfaces.* 2019;6(17):1900761. doi:10.1002/admi.201900761.

3. Kopecek J. Hydrogel biomaterials: a smart future? *Biomaterials.* 2007;28(34):5185-5192. doi:10.1016/j.biomaterials.2007.07.044.

4. Lee KY, Mooney DJ. Hydrogels for tissue engineering. *Chem Rev.* 2001;101(7):1869-1880. doi:10.1021/cr000108x.

5. Drury JL, Mooney DJ. Hydrogels for tissue engineering: scaffold design variables and applications. *Biomaterials.* 2003;24(24):4337-4351. doi:10.1016/s0142-9612(03)00340-5.

6. Li Z, Lin Z. Recent advances in polysaccharide-based hydrogels for synthesis and applications. *Aggregate.* 2021;2(2):e21. doi:10.1002/agt2.21.

7. Zhang H, Shi LWE, Zhou J. Recent developments of polysaccharide-based double-network hydrogels. *J Polym Sci.* 2022;61(1):7-43. doi:10.1002/pol.20220510.

8. Chen Q, Chen H, Zhu L, Zheng J. Fundamentals of double network hydrogels. *J Mater Chem B.* 2015;3(18):3654-3676. doi:10.1039/c5tb00123d.

9. Gaharwar AK, Peppas NA, Khademhosseini A. Nanocomposite hydrogels for biomedical applications. *Biotechnol Bioeng.* 2014;111(3):441-453. doi:10.1002/bit.25160.

10. Gomes ME, Rodrigues MT, Domingues RMA, Reis, RL. Tissue engineering and regenerative medicine: new trends and directions—a year in review. *Tissue Eng Part B Rev.* 2017;23(3):211-224. doi:10.1089/ten.TEB.2017.0081.

11. Liu C, Xu N, Zong Q, Yu J, Zhang P. Hydrogel prepared by 3D printing technology and its applications in the medical field. *Colloid Interface Sci Commun.* 2021;44:100498. doi:10.1016/j.colcom.2021.100498.

12. Bose S, Vahabzadeh S, Bandyopadhyay A. Bone tissue engineering using 3D printing. *Mater Today.* 2013;16(12):496-504. doi:10.1016/j.mattod.2013.11.017.

13. Li J, Wu C, Chu PK, Gelinsky M. 3D printing of hydrogels: rational design strategies and emerging biomedical applications. *Mater Sci Eng R Rep.* 2020;140:100543. doi:10.1016/j.mser.2020.100543.

14. Mani MP, Sadia M, Jaganathan SK, *et al.* A review on 3D printing in tissue engineering applications. *J Polym Eng.* 2022;42(3):243-265. doi:10.1515/polyeng-2021-0059.

15. Kirchmajer DM, Gorkin Iii R, in het Panhuis M. An overview of the suitability of hydrogel-forming polymers for extrusion-based 3D-printing. *J Mater Chem B.* 2015;3(20):4105-4117. doi:10.1039/c5tb00393h.

16. Xu W, Jambhulkar S, Zhu Y, *et al*. 3D printing for polymer/particle-based processing: a review. *Compos B Eng.* 2021;223:109102. doi:10.1016/j.compositesb.2021.109102.

17. Wei J, Wang J, Su S, *et al*. 3D printing of an extremely tough hydrogel. *RSC Adv.* 2015;5 (99):81324-81329. doi:10.1039/c5ra16362e.

18. Xu C, Dai G, Hong Y. Recent advances in high-strength and elastic hydrogels for 3D printing in biomedical applications. *Acta Biomater.* 2019;95:50-59. doi:10.1016/j.actbio.2019.05.032.

19. Jiang Z, Diggle B, Tan ML, Viktorova J, Bennett CW, Connal LA. Extrusion 3D printing of polymeric materials with advanced properties. *Adv Sci.* 2020;7(17):2001379. doi:10.1002/advs.202001379.

20. Díaz A, Herrada-Manchón H, Nunes J, *et al*. 3D printable dynamic hydrogel: as simple as it gets! *Macromol Rapid Commun.* 2022;43(21):2200449. doi:10.1002/marc.202200449.

21. Zhu Z, Wang Y-M, Yang J, Luo X-S. Hyaluronic acid: a versatile biomaterial in tissue engineering. *Plast Aesthetic Res.* 2017;4(12):219-227. doi:10.20517/2347-9264.2017.71.

22. Nair S, Remya NS, Remya S, Nair PD. A biodegradable in situ injectable hydrogel based on chitosan and oxidized hyaluronic acid for tissue engineering applications. *Carbohydr Polym.* 2011;85(4):838-844. doi:10.1016/j.carbpol.2011.04.004.

23. Jeon O, Song SJ, Lee K-J, *et al*. Mechanical properties and degradation behaviors of hyaluronic acid hydrogels cross-linked at various cross-linking densities. *Carbohydr Polym.* 2007;70(3):251-257. doi:10.1016/j.carbpol.2007.04.002.

24. Kim HS, Kim C, Lee KY. Three-dimensional bioprinting of polysaccharide-based self-healing hydrogels with dual cross-linking. *J Biomed Mater Res A.* 2022;110(4):761-772. doi:10.1002/jbm.a.37325.

25. Ouyang L, Highley CB, Rodell CB, Sun W, Burdick JA. 3D printing of shear-thinning hyaluronic acid hydrogels with secondary cross-linking. *ACS Biomater Sci Eng.* 2016;2(10):1743-1751. doi:10.1021/acsbiomaterials.6b00158.

26. Liu S, Liu X, Ren Y, *et al*. Mussel-inspired dual-cross-linking hyaluronic acid/epsilon-polylysine hydrogel with self-healing and antibacterial properties for wound healing. *ACS Appl Mater Interfaces.* 2020;12(25):27876-27888. doi:10.1021/acsami.0c00782.

27. Kim SW, Kim DY, Roh HH, Kim HS, Lee JW, Lee KY. Three-dimensional bioprinting of cell-laden constructs using polysaccharide-based self-healing hydrogels. *Biomacromolecules.* 2019;20(5):1860-1866. doi:10.1021/acs.biomac.8b01589.

28. Koivusalo L, Karvinen J, Sorsa E, *et al*. Hydrazone crosslinked hyaluronan-based hydrogels for therapeutic delivery of adipose stem cells to treat corneal defects. *Mater Sci Eng C.* 2018;85:68-78. doi:10.1016/j.msec.2017.12.013.

29. Jiang Y, Chen J, Deng C, Suuronen EJ, Zhong Z. Click hydrogels, microgels and nanogels: emerging platforms for drug delivery and tissue engineering. *Biomaterials.* 2014;35(18):4969-4985. doi:10.1016/j.biomaterials.2014.03.001

30. Ramimoghadam D, Eyckens DJ, Evans RA, Moad G, Holmes S, Simons R. Towards sustainable materials: a review of acylhydrazone chemistry for reversible polymers. *Chem Eur J.* 2024;30(49):e202401728. doi:10.1002/chem.202401728.

31. Hozumi T, Kageyama T, Ohta S, Fukuda J, Ito T. Injectable hydrogel with slow degradability composed of gelatin and hyaluronic acid cross-linked by Schiff's base formation. *Biomacromolecules.* 2018;19(2):288-297. doi:10.1021/acs.biomac.7b01133.

32. Oommen OP, Wang S, Kisiel M, Sloff M, Hilborn J, Varghese OP. Smart design of stable extracellular matrix mimetic hydrogel: synthesis, characterization, and in vitro and in vivo evaluation for tissue engineering. *Adv Funct Mater.* 2013;23(10):1273-1280. doi:10.1002/adfm.201201698.

33. Jeon O, Alt DS, Ahmed SM, Alsberg E. The effect of oxidation on the degradation of photocrosslinkable alginate hydrogels. *Biomaterials.* 2012;33(13):3503-3514. doi:10.1016/j.biomaterials.2012.01.041.

34. Kim HS, Kim JS, Hwang J, Lee IY, Lee KY. Decoupling stiffness and toughness of self-healing hydrogels for complex tissue regeneration via 3D bioprinting. *Chem Eng J.* 2024;487:150551. doi:10.1016/j.cej.2024.150551.

35. Mun CU, Kim HS, Kong M, Lee KY. Three-dimensional printing of hyaluronate-based self-healing ferrogel with enhanced stretchability. *Colloids Surf B Biointerfaces.* 2023;221:113004. doi:10.1016/j.colsurfb.2022.113004.

36. Wang S, Oommen OP, Yan H, Varghese OP. Mild and efficient strategy for site-selective aldehyde modification of glycosaminoglycans: tailoring hydrogels with tunable release of growth factor. *Biomacromolecules.* 2013;14(7):2427-2432. doi:10.1021/bm400612h.

37. Kafili G, Tamjid E, Simchi A. The impact of mechanical tuning on the printability of decellularized amniotic membrane bioinks for cell-laden bioprinting of soft tissue constructs. *Sci Rep.* 2024;14(1):29697. doi:10.1038/s41598-024-80973-3.

38. Kim JK, Srinivasan P, Kim JH, *et al*. Structural and antioxidant properties of gamma irradiated hyaluronic acid. *Food Chem.* 2008;109(4):763-770.

doi:10.1016/j.foodchem.2008.01.038.

39. Fan QG, Lewis DM, Tapley KN. Characterization of cellulose aldehyde using Fourier transform infrared spectroscopy. *J Appl Polym Sci.* 2001;82(5):1195-1202. doi:10.1002/app.1953.

40. Roh HH, Kim HS, Kim C, Lee KY. 3D printing of polysaccharide-based self-healing hydrogel reinforced with alginate for secondary cross-linking. *Biomedicines.* 2021;9(9):1224. doi:10.3390/biomedicines9091224.

41. Morgan FLC, Beeren IAO, Moroni L, Baker MB. Designing dynamic hydrogels: The interplay of cross-linker length, valency, and reaction kinetics in hydrazone-based networks. *Chem Mater.* 2025;37(8):2709–2719. doi:10.1021/acs.chemmater.4c02573.

42. Shin W, Chung K. Preparation and characterization of poly(acrylic acid)-based self-healing hydrogel for 3D shape fabrication via extrusion-based 3D printing. *Materials.* 2023;16(5):2085. doi:10.3390/ma16052085.

43. Karvinen J, Kellomäki M. 3D-bioprinting of self-healing hydrogels. *Eur Polym J.* 2024;209:112864. doi:10.1016/j.eurpolymj.2024.112864.

44. Stern R, Jedrzejas MJ. Hyaluronidases: their genomics, structures, and mechanisms of action. *Chem Rev.* 2006;106(3):818-839. doi:10.1021/cr050247k.

45. Lee HJ, Seo Y, Kim HS, Lee JW, Lee KY. Regulation of the viscoelastic properties of hyaluronate-alginate hybrid hydrogel as an injectable for chondrocyte delivery. *ACS Omega* 2020;5(25):15567-15575. doi:10.1021/acsomega.0c01763.

46. Allen JL, Cooke ME, Alliston T. ECM stiffness primes the TGFbeta pathway to promote chondrocyte differentiation. *Mol Biol Cell.* 2012;23(18):3731-3742. doi:10.1091/mbc.E12-03-0172.

47. Arora A, Kothari A, Katti DS. Pericellular plasma clot negates the influence of scaffold stiffness on chondrogenic differentiation. *Acta Biomater.* 2016;46:68-78. doi:10.1016/j.actbio.2016.09.038.